Proceedings of the 34th European Modeling & Simulation Symposium (EMSS), 015
19th International Multidisciplinary Modeling & Simulation Multiconference

ISSN 2724-0029 © 2022 The Authors.
doi: 10.46354/i3m.2022.emss.015

Electrostatic and Aerodynamic Modelling of the Charged Droplet Trajectories thanks to a Lagrangian-Eulerian Model in COMSOL Multiphysics®

Frédéric VIRY[1,*], Magali STURMA[2], Patrick NAMY[1] and Bruno BARBET[2]

[1]SIMTEC, 5 rue Félix Poulat, 38000 Grenoble, France
[2]MARKEM-IMAJE, 9 rue Gaspard Monge, 26500 Bourg-lès-Valence, France

*Corresponding author. Email address: frederic.viry@simtecsolution.fr

Abstract

In the field of industrial marking, continuous inkjet technology is based on high speed emission of ink drops. The printing quality is directly linked to the interactions of the droplets with their environment during flight time: electric field, aerodynamic perturbations, and droplet-droplet interactions. To model all the physics, a fully coupled model is developed within COMSOL Multiphysics®. Dynamics of droplets are modelled by coupling a particle tracing approach – lagrangian approach – to a continuous eulerian one. For the particle dynamics, the Coulomb force, the Lorentz force and the drag forces, dependent on the air velocity, are considered. The surrounding air is itself driven by the movement of the other droplets, and is modelled by the Navier-Stokes equation in an eulerian approach. This paper shows the development of a continuous inkjet printhead so called digital twin, providing a decision-making tool to ensure the stability of the ink raster.

Keywords: Droplet modelling; fluid-particle interaction; continuous inkjet

1. Introduction

In the area of Continuous Inkjet technology (CIJ), the printing quality is based on the accuracy of droplets placement on a moving media. Electrically charged droplets are emitted at high speed (20 m/s, 100 kHz) and their positions are mainly controlled by the breakoff quality and the droplets deflection. This article focuses on the last item. The droplet deflection depends on the electric field at the first order, and on aerodynamic perturbations, and droplet-droplet interactions at the second order (Martin, Hoath, & Hutchings, 2008). All these effects are modelled within COMSOL Multiphysics® (COMSOL, 2020), in order to get a prediction of the droplets trajectories and locations on the printed media. The results provided by simulations are compared to experimental tests to validate the model and make it a design support tool.

2. State of the Art

The main forces acting on droplets are the Lorentz force, the Coulomb force and aerodynamic forces (Matsumoto, Inoue, & Matsuno, 1999) (Martin, Hoath, & Hutchings, 2008) (Ikegawa, Eiji, Harada, & Takagishi, 2014).

In (Matsumoto, Inoue, & Matsuno, 1999), approximations of the aerodynamic forces are obtained analytically under simplifying hypotheses depending on empirical coefficients.

In (Ikegawa, Eiji, Harada, & Takagishi, 2014), the authors proposed to model and simulate the aerodynamic interactions using a full Lagrangian multi-phase approach.

In (Sturma, Namy, Bruyère, & Barbet, 2020), a 2D

numerical model taking into account the Lorentz force and Coulomb forces was proposed, allowing to predict the droplets final position on the printed media with a certain bias, attributed to the lack of taking of consideration of aerodynamic effects. This paper is an extension of this work (Sturma, Namy, Bruyère, & Barbet, 2020) in 3 dimensions and with droplet/air flow coupling. With the third dimension, out-of-plane deviations of the droplets due to the destabilizing electrostatic repulsion, but also the induced out-of-plane air motion are taken into account. Compared to (Ikegawa, Eiji, Harada, & Takagishi, 2014), the novelty of this work is taking into account aerodynamic interactions in a Lagrangian-Eulerian framework.

3. Materials and Methods

3.1. Physical process description

The droplet generator builds a stream of charged and non-charged droplets of diameter d (typically 100 µm) and mass m (typically less than 1 µg), propelled from the nozzle at high frequency f_{jet} (typically 100 kHz) and velocity v_{jet} (typically 20 m/s) along the y-axis towards the gutter, and passes between two deflection electrodes creating an electrostatic field $\boldsymbol{E}$ (typically 1 kV/mm between electrodes), where charged droplets of charge q (typically 1 pC) are more or less deviated depending their electrical charge (Lorentz force), while non-charged droplets are gathered in a gutter and recycled in the ink circuit (Fig. 1). Charged droplets repulse two-by-two by electrostatic repulsion (Coulomb force). Non-charged droplets create a wake maintaining to a certain extent the stream velocity (drag force), and may be used to artificially extend the distance between charged droplets, minimizing their electrostatic repulsion.

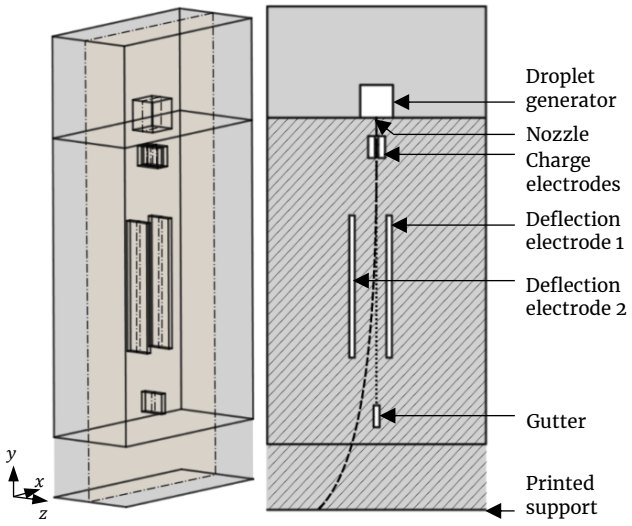

Figure 1. Schematic representation of print head and the simulation domain. Head is a few millimeters above the printed media. In the right hand side, the grey domain represents the domain where the electric field is computed, the hatched domain represents the domain where droplets evolve and where Navier-Stokes equations are solved, and lines represent typical trajectories of droplets: the dotted one in the non-charged case, the dashed one in the charged case.

3.2. Experimental Setup

The experimental bench is the same as the one described in (Sturma, Namy, Bruyère, & Barbet, 2020). It is built with a commercial continuous inkjet printer (Markem-Imaje 9450 brand name) and a customized printhead used to change velocity and frequency of droplets and the voltage of the deflection electrode. A strobe light synchronized on droplets frequency is added to monitor droplets positions during flight thanks to a micrometric table controller (Fig. 2.a). By this way, measurements of the deviation amplitude of charged droplets submitted to the electric field, and distances between droplets are available at a certain frequency. So far, the velocity of droplets is available in the jet (Fig. 2.b).

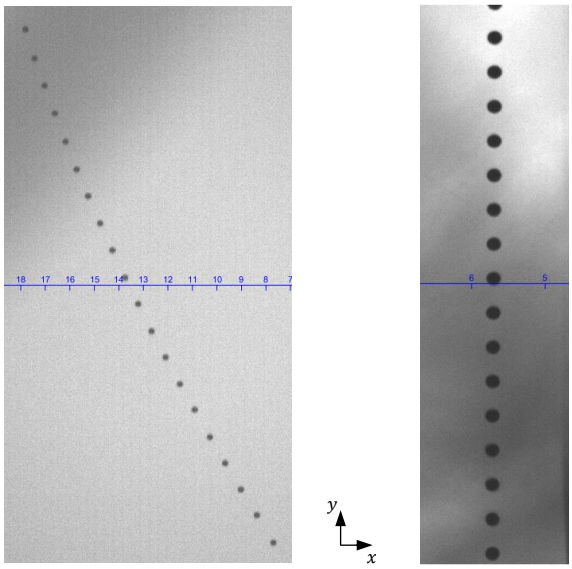

(a) Charged droplets raster deviated by the electric field in flight.

(b) Non-charged droplets in the jet axis.

Figure 2. Snapshots of positions of charged and non-charged droplets.

3.3. Numerical Model

3.3.1. *Electric Field*

In the print head, the electric field is controlled by imposing the electric potential of conductive parts. These potentials are kept constant while printing. The electric potential V is obtained by solving the Laplace equation with appropriate boundary conditions (Fig. 1, grey domain):

$$\Delta V = 0. \tag{1}$$

The surfaces of the droplet generator, the charge electrodes, and the gutter are kept to $V = 0$. The electric potential of electrodes 1 and 2 are -4000 V and 4000 V,

respectively. Homogeneous Neumann conditions are imposed on the remaining boundaries of the domain (bounding box), modelling electrical isolation. The electric field $\boldsymbol{E}$ is then obtained as follows:

$$\boldsymbol{E} = -\boldsymbol{\nabla} V. \tag{2}$$

3.3.2. Droplet Dynamic and Air Flow

The droplets are modelled punctually in a lagrangian framework, due to the very small size of droplets compared to the characteristic distance between the print head parts (typically 1 cm). Once propelled from the nozzle, the position $\boldsymbol{x}_i$ and the velocity $\boldsymbol{v}_i$ of a droplet is computed through the fundamental principle of dynamics:

$$m\,\frac{d\boldsymbol{v}_i}{dt} = \boldsymbol{F}_l(i) + \boldsymbol{F}_c(i) + \boldsymbol{F}_g(i) + \boldsymbol{F}_d(i). \tag{3}$$

where indexes denote the droplet numbers, $\boldsymbol{F}_l$ the Lorentz force:

$$\boldsymbol{F}_l(i) = q_i\,\boldsymbol{E}(\boldsymbol{x}_i), \tag{4}$$

$\boldsymbol{F}_c$ the Coulomb force between all charged droplets:

$$\boldsymbol{F}_c(i) = \frac{1}{4\pi\varepsilon_0}\sum_{j=1}^{N} q_i\,q_j\,\frac{\boldsymbol{x}_i - \boldsymbol{x}_j}{\left|\boldsymbol{x}_i - \boldsymbol{x}_j\right|^3}, \tag{5}$$

$\boldsymbol{F}_g$ the gravity force, which can be neglected against other forces exerted on droplets because of their lightness. Finally, $\boldsymbol{F}_d$ denotes the drag force caused by friction between a droplet and air:

$$\boldsymbol{F}_d(i) = f(i)\cdot(\boldsymbol{u}(\boldsymbol{x}_i) - \boldsymbol{v}_i) \tag{6}$$

where $\boldsymbol{u}$ is the air velocity field, and f is a friction coefficient given by the Schiller-Naumann drag law (COMSOL, 2020):

$$\begin{aligned} f(i) &= 3\,\pi\,\mu\,d\,(1 + 0.15\cdot[R_e(i)]^{0.687}) \\ R_e(i) &= \frac{\rho\,d\,|\boldsymbol{u}(\boldsymbol{x}_i) - \boldsymbol{v}(\boldsymbol{x}_i)|}{\mu} \end{aligned} \tag{7}$$

where ρ denotes the air density, 1.20 kg/m^3, and μ the air dynamic viscosity, $1.81{\cdot}10^{-5}$ Pa·s. This drag law is adapted for Reynolds numbers less than 10^3 (COMSOL, 2020).

The Mach number never exceeds 0.1 and the Reynolds number is approximatively 10^2 maximum, so the air flow is modelled by the incompressible Navier-Stokes equations (Fig. 1, hatched domain):

$$\begin{aligned} \boldsymbol{\nabla}\cdot\boldsymbol{u} &= 0 \\ \rho\left(\frac{\partial\boldsymbol{u}}{\partial t} + \boldsymbol{u}\cdot\boldsymbol{\nabla}\boldsymbol{u}\right) &= -\boldsymbol{\nabla}p + \boldsymbol{\nabla}\cdot[\mu(\boldsymbol{\nabla}\boldsymbol{u} + (\boldsymbol{\nabla}\boldsymbol{u})^{\mathrm{T}})] + \boldsymbol{f}_v \end{aligned} \tag{8}$$

where $\boldsymbol{u}$ denotes the air velocity, p the air pressure, ρ and μ have been introduced before, and $\boldsymbol{f}_v$ is a volumetric force in reaction to the friction force between air and droplets:

$$\boldsymbol{f}_v = -\sum_{i=1}^{N} \boldsymbol{F}_d(i)\;\delta_{\boldsymbol{x}_j} \tag{9}$$

with δ, the Dirac distribution. No-slip boundary conditions are used on the surface of parts of the print head, and open boundary conditions are considered to model a non-limited area. Initially, the air is at rest.

3.3.3. Numerical Implementation

This model is implemented within COMSOL Multiphysics® 5.6. All eulerian variables are spatially discretized using finite-elements and the same mesh is used for both electrostatics and air flow (Fig. 3).

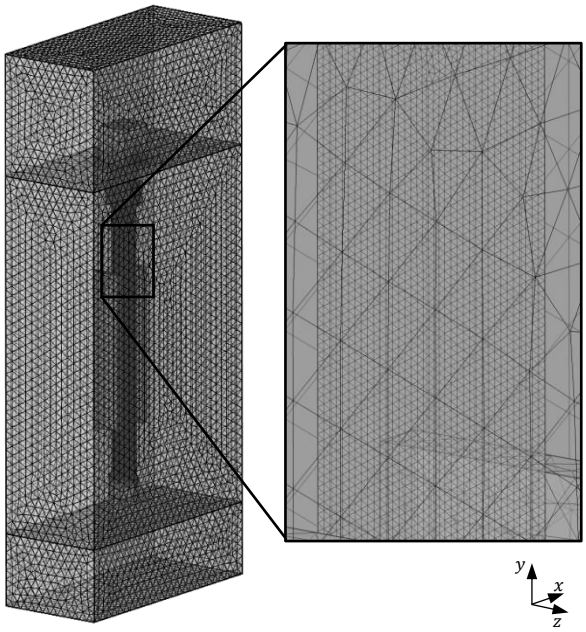

Figure 3. Surface mesh representation. The mesh is refined at the expected location of non-charged droplets to ensure a high resolution of the wake.

In Eq. 1, V is discretized with $P2$-elements, leading to 1.6 million of degrees of freedom.

Air flow variables $\boldsymbol{u}$ and p are spatially discretized using stabilized $P1+P1$ finite elements (Hughes, Franca, & Balestra, 1986), leading to 0.8 million of degrees of freedom to solve at each timestep.

The time discretization and resolution are performed by a generalized-α solver. A each timestep, a set of nonlinear equations is solved for discrete representations of $(\boldsymbol{u}, p)$ and $\boldsymbol{x}$. A *segregated* scheme is used, which consists in performing multiple iterations in an *outer loop* until convergence where: (1) solve the position of the droplets until convergence by Newton' iteration in an *inner loop* and (2) solve the set of linearized equations of the air flow. The outer loop is stopped when convergence is met using an error norm taking into account both eulerian $(\boldsymbol{u}, p)$ and lagrangian $\boldsymbol{x}$ variables. Mixing both types of variables in this error

estimation is not desirable, as their norms are not comparable. Thanks to the segregated scheme, convergence tests are performed separately on eulerian and lagrangian variables, which is much safer numerically. Such scheme has shown a good tradeoff between computational performance and physical realism.

4. Results and Discussion

4.1. Drag Force

A first model-experiment comparison aims to check the validity of the drag law Eq. 6-7. Droplets have the same size and the same mass for both experimental bench and numerical model.

In this case, no electric field is taken into account and a single droplet is slowed down by its surrounding air.

In Fig. 4, the velocity of the droplet is represented along the axis of the trajectory for both experiment and numerical model. The origin of this axis is chosen for both as the position where the droplet has a velocity about 18 m/s. Experimental velocities are obtained by finite differences from position measurements.

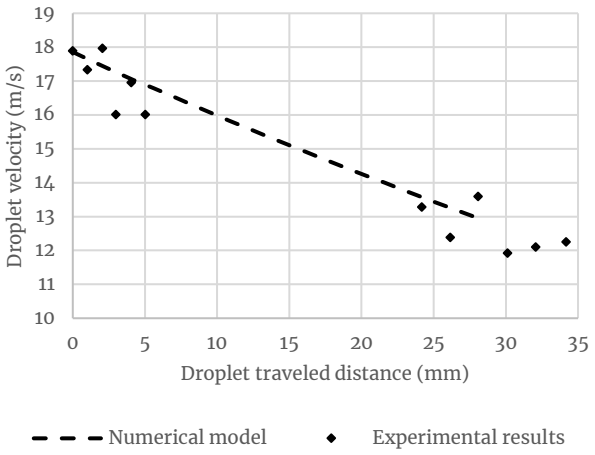

Figure 4. Model-experiment comparison of the droplet velocity along a straight trajectory.

Fig. 4 shows a good agreement between numerical model and experimental velocities up to experimental errors. The comparisons are performed in the regime where the highest order of magnitude of relative velocity between the droplet and air is attained, *i.e.* within the highest range of Reynolds number encountered in the model. The Schiller-Naumann law seems therefore well-suited to model the air-droplet aeraulic interaction.

4.2. Non-Charged Droplets Wake

A second model-experiment comparison is performed, to study a full droplet/air flow coupling. In this setup, droplets have the same size and the same mass, and are propelled at the same frequency and velocity, for both experimental bench and numerical model.

Fig. 5 shows the velocity of non-charged droplets versus the distance to the nozzle measured experimentally and computed numerically.

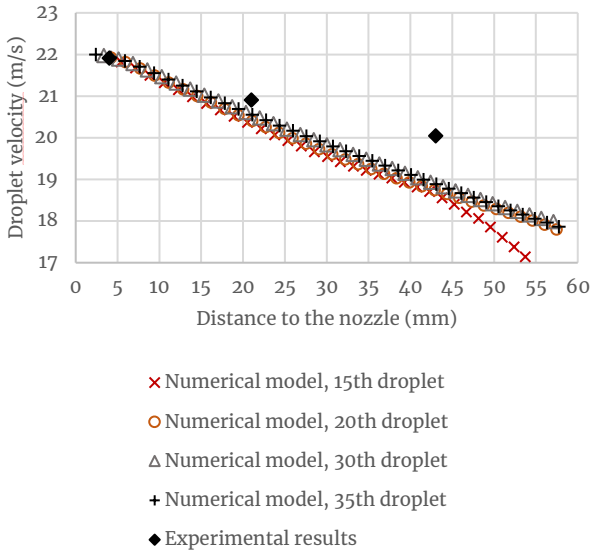

Figure 5. Model-experiment comparison of the droplet velocity within the non-charged droplets wake at near-stationary state.

Fig. 5 shows that the velocity of the droplets only depends on their position after only 20 droplets, showing that (1) the model is able to reach a stationary state with non-charged droplets and (2) this stationary state is reached after a few tens of non-charged droplets. This second result is important in terms of computational costs, since it is not needed to simulate the trajectory of thousands of non-charged droplets before simulating a printing scenario with charged droplets. Identically to experimental results, droplets undergo a velocity decrease. This decrease is overestimated in the numerical model, which may lead to inaccuracies in the final position of charged droplets. The gap between model and experiment may be explained by the fact that the gutter is slightly depressurized on the experimental bench, which may lead to air aspiration from the nozzle towards the gutter, and then to higher velocities in the stream of non-charged droplets. The gutter depressurization is not taken into account in the numerical model, and is part of ongoing work.

4.3. Effects of Friction Force and Air Motion

A full simulation of a printing scenario is performed. Fig. 6.a. show the electric field within the head. The simulated printing scenario is a raster of 24 charged droplets, each one separated by one non-charged droplet. This sequence is preceded by a sequence 60 non-charged droplets. A snapshot of the trajectory of the droplets and air flow is shown in Fig. 6.b.

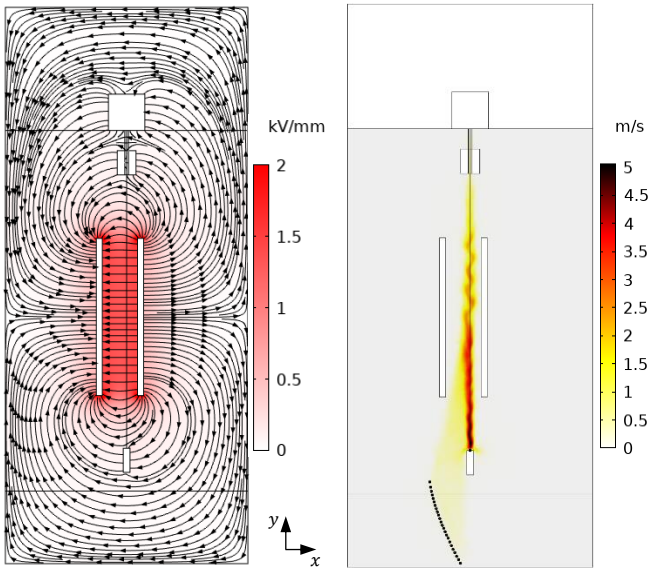

(a) Electric field magnitude and Lorentz force field.

(b) Snapshot of the trajectory of the droplets and air velocity magnitude.

Figure 6. Example of simulated trajectory of droplets with the numerical model.

In order to quantify the effect of coupling the dynamics of the droplets and air through a friction force, a simulation of the same scenario has been performed by disabling the drag force (Eq. 6-7) and air flow (Eq. 8-9), mimicking in 3D the behavior of the state-of-the-art model (Sturma, Namy, Bruyère, & Barbet, 2020). The final position of charged droplets on the printed support and raster height are quantified in Table 1 for both models.

Table 1. Comparison of the absolute deflection of droplets and raster height in x-direction for both models (unit: mm). The origin of the measurement is the intersection between the axial trajectory of non-charged droplets and the printed support plane.

Model	Droplet 1	Droplet 24	Raster height
Drag and air flow disabled	1.48	8.87	7.39
Drag and air flow enabled	1.62	10.29	8.67

On this printing scenario, the droplet/air flow coupling leads to an increase of 15% on the raster height, but more generally to a larger deflection of charged droplets. This result is not surprising, since friction leads to a longer residence time of droplets between deflection electrodes, resulting in a larger effect of the electric field in the x-direction. This demonstrates the importance of taking into account this effect to ensure the predictability of the numerical model.

5. Conclusions

A model has been developed to predict the trajectory and the final position on a printed support of a stream of charged and non-charged droplets in a continuous inkjet print head. Simulating a printing scenario consists in first computing an electrostatic field aiming to deviate charges from a straight trajectory, and second computing the flight of a stream of droplets. During the flight of the charged droplets, the model takes into account both the effect of the electric field and the two-by-two electrostatic interactions, as in the state-of-the-art model. The major contributions of this work are the change from a 2D approach to a 3D one to take into account out-of-plane deviations of the droplets, and to consider the air flow and friction force using the Schiller-Naumann drag law.

The predictability of the approach has been assessed through model-experiment comparisons: (1) the relevance of the Schiller-Naumann drag law in the typical range of Reynolds number experienced by air around a droplet, and (2) the capability of the model to predict the near-stationary state of a stream of non-charged droplets. For this latter point, the numerical model overestimates the velocity decrease in the wake, and solving this bias is part of ongoing work. Computationally, this new approach comes with a higher cost than the state-of-the-art model. Still, it is shown that only a few tens of non-charged droplets are needed to attain their near-stationary state, proving the affordability of simulating continuous inkjet marking with our numerical model. Finally, the interest of our contribution has been assessed on a realistic test-case, where enabling the droplet/air flow coupling results in an increase of 15% the raster height on the printed support, which demonstrates the importance of the effect.

This model is currently used as a design support tool: it is used to identify the effect of combined design parameters on the printing quality, aiming to derive conception rules.

Funding

This work has been founded by MARKEM-IMAJE and made in a fruitful collaboration between MARKEM-IMAJE and SIMTEC.

Acknowledgements

The authors thank gratefully Jean-Marie Rolland and René Ferry for their experimental measurements and their expertise on the subject.

References

COMSOL. (2020). COMSOL Multiphysics® v. 5.6. www.comsol.com. Stockholm, Sweden.

COMSOL. (2020). Other Drag Laws, Schiller-Naumann. In COMSOL, *Particle Tracing Module, User's Guide, COMSOL 5.6* (p. 270).

Hughes, T. J., Franca, L. P., & Balestra, M. (1986, November). A new finite element formulation for

computational fluid dynamics: V. Circumventing the babuška-brezzi condition: a stable Petrov-Galerkin formulation of the stokes problem accommodating equal-order interpolations. *Computer Methods in Applied Mechanics and Engineering, 59*(1), 85-99.

Ikegawa, M., Eiji, I., Harada, N., & Takagishi, T. (2014). Development of Ink-Particle Flight Simulation for Continuous Inkjet Printer. *Journal of Manufacturing Science and Engineering, 136*(5).

Martin, G. D., Hoath, S. D., & Hutchings, I. M. (2008). Inkjet Printing - The Physics of Manipulating Liquid jets and Drops. *Journal of Physics: Conference Series, 105.*

Matsumoto, S., Inoue, T., & Matsuno, J. (1999). Flight Stability of Droplets in an Electrostatic Ink-Jet Printer. *Recent Progress in Ink Jet Technologies II*, 280-285.

Sturma, M., Namy, P., Bruyère, V., & Barbet, B. (2020). Modeling of charged droplet dynamics in an Electric Field using COMSOL Multiphysics®. *COMSOL Conference 2020 Europe.*